Received: 25 November 2020 | Revised: 15 March 2021 | Accepted: 4 May 2021

DOI: 10.1002/met.2002

Meteorological Applications
Science and Technology for Weather and Climate
Open Access
RMetS

REVIEW ARTICLE

Calibration of non-catching precipitation measurement instruments: A review

L. G. Lanza[1,2] | A. Merlone[3] | A. Cauteruccio[1,2] | E. Chinchella[1,2] | M. Stagnaro[1,2] | M. Dobre[4] | M. C. Garcia Izquierdo[5] | J. Nielsen[6] | H. Kjeldsen[6] | Y. A. Roulet[7] | G. Coppa[3] | C. Musacchio[3] | C. Bordianu[8] | M. Parrondo[5]

[1]Department of Civil, Chemical and Environmental Engineering, University of Genova, Genoa, Italy

[2]WMO/CIMO Lead Centre 'B. Castelli' on Precipitation Intensity, Italy

[3]Istituto Nazionale di Ricerca Metrologica, Applied Thermodynamics Program, Torino, Italy

[4]Federal Public Service Economy, Metrology, National Standards, Belgium

[5]Centro Español de Metrología, Tres Cantos (Madrid), Spain

[6]Danish Technological Institute, Aarhus, Denmark

[7]Federal Office of Meteorology and Climatology MeteoSwiss, Payerne, Switzerland

[8]National Metrology Institute of the Republic of Moldova, Chisinau, Moldova

Correspondence
C. Musacchio, Istituto Nazionale di Ricerca Metrologica, Applied Thermodynamics Program, Torino, Italy.
Email: c.musacchio@inrim.it

Funding information
European Union's Horizon 2020; EMPIR

Abstract

Non-catching type gauges are the emerging class of in situ precipitation measurement instruments. For these instruments, rigorous testing and calibration are more challenging than for traditional gauges. Hydrometeors characteristics like particle size, shape, fall velocity and density must be reproduced in a controlled environment to provide the reference precipitation, instead of the equivalent water flow used for catching-type gauges. They are generally calibrated by the manufacturers using internal procedures developed for the specific technology employed. No agreed methodology exists, and the adopted procedures are rarely traceable to internationally recognized standards. The EURAMET project 18NRM03 'INCIPIT' on 'Calibration and accuracy of non-catching instruments to measure liquid/solid atmospheric precipitation', funded by the European Metrology Programme for Innovation and Research (EMPIR), was initiated in 2019 to investigate calibration and accuracy issues of non-catching measuring instruments used for liquid/solid atmospheric precipitation measurement. A survey of the existing models of non-catching type instruments was initially performed and this paper provides an overview and a description of their working principles and the adopted calibration procedures. Both literature works and technical manuals disclosed by manufacturers are summarized and discussed, while current limitations and metrological requirements are identified.

KEYWORDS

calibration, hydro-meteorology, meteomet, non-catching gauges, precipitation, precipitation measurement and analysis, uncertainty analysis, verification

1 | INTRODUCTION

The development of highly accurate precipitation gauges for both liquid and solid precipitation is an increasingly relevant and pressing requirement in the environmental sciences and their applications (Lanza & Stagi, 2008). Non-catching type instruments, which do not use a container to collect the hydrometeors when approaching the

ground, are the emerging class of in situ precipitation gauges (Cauteruccio et al., 2021a). They detect the microphysical and dynamic characteristics of single or multiple hydrometeors while these cross a given section, or a volume, of the atmosphere (or directly impact the sensor) by employing optical, acoustic and microwave principles.

National Meteorological and Hydrological Services (NMHSs) and other organizations, in charge of the management of observation networks over large regions, increasingly look at such kind of instruments as a potential improvement over the more traditional catching-type gauges (typically tipping-bucket and weighing gauges), notwithstanding the higher lifecycle cost. The reasons are their potential in reducing the maintenance burden (by eliminating any moving part or containers to be periodically emptied and serviced), the high temporal resolution, the large number of parameters provided and their suitability to be part of a fully automated observation network. Drawbacks can be easily identified in the higher complexity of the exploited technology, so that the capability of the user to correctly manipulate, maintain and calibrate the instrument may be limited.

Non-catching type instruments are generally calibrated by the manufacturers, using internal procedures developed for the specific technology employed. No widely agreed procedure – nor any documentary standard – exists within national or international institutions. The adopted procedures are rarely traceable to the International System of Units (SI), and are often not even reproducible. Limited information is generally provided by the manufacturers about the methodology and instrumentation adopted for calibration purposes.

Having no funnel to collect the rainwater, traceable calibration and uncertainty evaluation for non-catching gauges are more difficult than for catching-type gauges, and the use of an equivalent, reference flow rate (see e.g. Colli et al., 2014) is not possible. Rather, for an appropriate metrological characterization of non-catching instruments, the actual rain event characteristics must be reproduced, including particle size distribution (PSD), shape, density and fall velocity. A considerable metrological effort is therefore required to resolve traceability and uncertainty issues and to support new calibration methods including the development of standardized laboratory rainfall generators.

As regards solid precipitation, non-catching type instruments were included in the recent WMO SPICE (solid precipitation inter-comparison experiment, WMO, 2012) and compared with gauge measurements in a DFIR (double fence inter-comparison reference) at various test sites (Nitu et al., 2018). The study concluded that further analysis is needed to better understand the behaviour of non-contact type measurement instruments, especially working with the raw data (drop size and fall speed distribution), and exploiting the full capacity of such devices, which can provide much more information than the precipitation accumulation (precipitation type, SYNOP and METAR codes, etc.). Field tests on SPICE reference sites have been continued in that sense after the official end of the project (Smith et al., 2020) to enhance the knowledge on the operational use of non-catching type instruments in winter conditions.

For liquid precipitation measurements, the evidence from the last WMO inter-comparison of rainfall intensity (RI) gauges in the field (Vuerich et al., 2009) is that, due to calibration issues, caution should be posed in using the information obtained from non-catching instruments in any real-world application and in assessing the results of scientific investigations based on such measurements.

The main effort to develop standard procedures for the calibration of precipitation measurement instruments is presently being performed at the European level. The first experience was the development of the Italian national standard UNI 11452:2012, and the follow-up extension of such initiative at the European scale, leading to the publication of the recent standard EN 17277:2019. The scope of this standard is however limited to catching-type gauges, which – due to the presence of the rain collector – can be calibrated using a known and constant flow rate generated in the laboratory as the reference (Santana et al., 2015). Traceable instrument calibration methods for non-catching gauges is the next step of the ongoing normative effort at the European scale under CEN TC318/WG12, but various scientific and methodological aspects are still open issues.

The project MeteoMet (Merlone et al., 2015), funded under the European Metrology Research Programme (EMRP), initiated a series of experimental activities in metrology for meteorology, with the MeteoMet2 (Merlone et al., 2018) specifically addressing the issue of atmospheric precipitation measurements from a metrological perspective. An associated research grant focused on rainfall measurements using catching and non-catching gauges. It is under this framework that, to support the ongoing normative effort, the INCIPIT project 'Calibration and accuracy of non-catching instruments to measure liquid/solid atmospheric precipitation' was initiated in July 2019 (Merlone et al., 2020a). The project aims at introducing metrological soundness, reproducibility and standardization in the calibration of non-catching type instruments, so that an uncertainty budget can be determined, and measurements made traceable to the SI. The rigorous metrological approach based on modelling the measurement process and expressing the influence parameters in a model function will be implemented, taking into account different types of rain

gauges and the different calibration schemes. By developing, characterizing, testing and comparing different types of rain generators, test calibrations of a representative number of different non-catching rain gauges will be performed. A calibration procedure will be studied, developed and validated by comparing the different systems and methods. The procedures, in terms of guideline proposal, will be submitted to the chief stakeholder, the World Meteorological Organisation (WMO) and CEN TC318/WG12, for uptake in documentary standards.

2 | RELEVANT CHARACTERISTICS OF ATMOSPHERIC PRECIPITATION

The World Meteorological Organisation (WMO), in its Guide to Meteorological Instruments and Methods of Observation (WMO, 2018), defines atmospheric precipitation as '*the liquid or solid products of the condensation of water vapour falling from clouds, in the form of rain, drizzle, snow, snow grains, snow pellets, hail and ice pellets; or falling from clear air in the form of diamond dust*'. Hydrometeors falling through the atmosphere can have different size, shape, velocity (magnitude and components) and density. The precipitation intensity (usually indicated as snowfall intensity, SI, for solid and rainfall intensity, RI, for liquid precipitation) and the associated PSD are two main factors used to characterize a precipitation event, independently from the measurement principle. The precipitation intensity is defined in the same Guide as '*the amount of precipitation collected per unit time interval*' (although the term 'collected' would be applicable to catching gauges only), while the PSD, usually indicated with $N(d)$ and expressed in (L^{-3} L^{-1}), provides the number of particles (liquid or solid) per unit volume of air and per unit size interval having a volume equal to the sphere of diameter comprised between d and $d + dd$. This section of the review is taken from the PhD thesis work of Cauteruccio (2020).

2.1 | Particle size distribution

The PSD is usually depicted in a (d, $N(d)$) semi-logarithmic plot. A universal formulation that can describe in an easy way the high variability of PSDs in nature, influenced by the regional and seasonal climatology and processes governing the formation of hydrometeors in the atmosphere, is not available. Information about the PSD comes from observations and is therefore subject to uncertainties that are rarely quantified.

Two formulations for the PSD are commonly used in the literature, the Exponential (Marshall & Palmer, 1948) and the Gamma (Ulbrich, 1983) distributions. By fitting experimental observations obtained using dyed filter paper (Marshall et al., 1947), Marshall and Palmer (1948) provided the exponential form of the PSD as follows:

$$N(d) = N_0 e^{-\Lambda d}, \tag{1}$$

where N_0 and Λ are two suitable parameters, with N_0 (L^{-1} L^{-3}) as the intercept and Λ (L^{-1}) as the slope of the linear form of this curve in a semi-log plot.

Marshall and Palmer, for a widespread mid-latitude rain, found a constant value $N_0 = 8000$ ($mm^{-1}m^{-3}$) and a relationship for Λ, as a function of the RI, as reported in Equation (2).

$$\Lambda = 41\,\mathrm{RI}^{-0.21}\left(\mathrm{cm}^{-1}\right). \tag{2}$$

This distribution is valid for stratiform precipitations and has the tendency to overestimate the concentration of small drops (typically under 0.5 mm). Indeed, these droplets cannot fall if there is upward wind and tend to evaporate when they enter non-saturated air. Integration of this distribution between 0.5 and 6 mm for a rainfall rate of, for example, 5 mm h^{-1} gives a total concentration of drops of 6.4×10^{-4} (cm^{-3}). This means that there are typically between 100 and 1000 drops/m^3 during stratiform rain, corresponding to an approximate distance between drops of 20 and 10 cm.

Waldvogel (1974), by measuring the distribution of raindrops with an electro-acoustic device (see functioning description in Section 3.2.1) and by means of a radar reflectivity analysis, for different types of precipitation (showers, thunderstorms and widespread rain), showed that the parameter N_0 is not constant and can change abruptly because it is a function of the convection activity in the clouds. He called this phenomenon '*The N_0 jump*'. Radar measurements indicated that the N_0 *jump* occurred when one of the mesoscale convective areas moved in or out of the region above the station, which means that the situation changed from uniform (widespread rain) to convective (shower or thunderstorm) or vice versa.

For very small drop diameters (below 1 mm) the $N(d)$ values decrease while decreasing the particle diameter, therefore, a downward concavity of the PSD is obtained. Currently, it is not clear whether this characteristic is ascribable to the limitation of the measuring instruments to detect very small particles or it is physically based. Moreover, some disdrometers, especially radars, provide

higher $N(d)$ values for small diameters causing an upward concavity in the distribution.

Ulbrich (1983) proposed the Gamma distribution in the form:

$$N(d) = N_0 d^{\mu} e^{-\Lambda d}, \tag{3}$$

where the exponent μ is the shape parameter and can have positive or negative values and the intercept N_0 is in $\mathrm{mm}^{-1-\mu}\mathrm{m}^{-3}$, d in mm, when $N(d)$ is expressed in $\mathrm{mm}^{-1}\mathrm{m}^{-3}$.

Ulbrich summarized experimental observations reported by other authors including Mueller (1965), Caton (1966) and Blanchard (1953). In the work of Mueller, a variety of rainfall types including continuous rain, showers and thunderstorms were observed and for all of them the observed PSDs are concave downward. When fitted with the gamma formulation, these PSDs would have $\mu > 0$. Almost all Caton's PSDs are similar to those reported by Mueller and can be described by a Gamma distribution with $\mu > 0$. Differently, orographic precipitation, as observed by Blanchard, is characterized by many small-size drops. This type of precipitation events can be described by a Gamma distribution with $\mu < 0$. In addition, Ulbrich conducted a theoretical analysis with the aim to describe the modification of the distribution from the exponential form to a concave shape. The author affirmed that the variation in N_0 is independent from the variation of Λ while a direct relationship between N_0 and μ exists in the form:

$$N_0 = 6 * 10^4 e^{3.2\mu} \left(\mathrm{cm}^{-1-\mu}\mathrm{m}^{-3}\right). \tag{4}$$

The work of Caracciolo et al. (2008) is based on rain events measured in the Italian territory by employing radar and two different types of disdrometers (Joss-Waldvogel and Pludix) with a sampling time of 1 min. Each 1-min PSD value was classified into one out of six categories, based on the measured liquid precipitation intensity (RI). Two examples of the average observed PSD data collected in Florence (Italy) obtained by the Joss-Waldvogel and Pludix disdrometers are reported in Figure 1, where the minimum diameter observed by the Pludix is 1 mm while the Joss-Waldvogel also reports data for $d < 1$ mm. It is useful to observe that, for the same region and precipitation rate category, different PSD values were obtained by the two instruments, especially in the case of higher precipitation intensity, showing also an opposite trend for hydrometeors of $d < 2$ mm.

As for solid precipitation, in the work of Houze Jr et al. (1979), the parameters of the Marshall-Palmer distribution (Equation 1) were derived as a function of the air temperature from measurements in frontal clouds obtained using an optical particle spectrometer. The temperature at flight altitude during the probe measurements ranged from −42 to +6°C. Results showed that both N_0 and Λ decrease with increasing T and a sudden 'jump' of the Λ value occurred for $T > 0$°C when aggregated snow particles melt to much smaller and faster falling drops.

2.2 | Terminal velocity

Because drops fall from a high altitude, they reach the ground with their terminal velocity. The terminal velocity, w_T, is defined as the maximum velocity attainable by an object as it falls through a fluid. This condition is reached when the sum of the drag force and the buoyancy force is equal to the downward force of gravity acting on the object. In these conditions, the motion of the object is no more accelerated.

As reported in various literature works where hydrometeor trajectories are modelled (see e.g. Colli et al., 2016; Nešpor & Sevruk, 1999; Thériault et al., 2012, 2015), the motion of a falling particle in the atmosphere is described by the following equation:

$$\rho_p V_p \boldsymbol{a}_{\mathrm{p}} = -\frac{1}{2} C_D A_p \rho_a \left(\mathbf{v}_p - \mathbf{v}_a\right)\left|\mathbf{v}_p - \mathbf{v}_a\right| + V_p\left(\rho_a - \rho_p\right)\mathbf{g}, \tag{5}$$

where $\boldsymbol{a}_{\mathrm{p}}$ is the particle acceleration, $\mathbf{v}_a$ and $\mathbf{v}_p$ are the velocity vectors of the air and the particle, $\mathbf{g}$ is the acceleration of gravity, C_D is the drag coefficient, A_p is the particle cross-section area and ρ_a and ρ_p are the density of the air and the particle. Equation (5) is written assuming an upward positive orientation of the z-axis, while the velocity and acceleration components are positive in the positive direction of the related axes. The quantity $\mathbf{v}_p - \mathbf{v}_a$ is the relative particle-to-air velocity.

The vertical component of Equation (6) becomes:

$$a_{\mathrm{pz}} = -\frac{1}{2} C_D A_p \frac{\rho_a}{\rho_p V_p}\left(\mathrm{w}_p - \mathrm{w}_a\right)\left|\mathbf{v}_p - \mathbf{v}_a\right| + \frac{\left(\rho_p - \rho_a\right)}{\rho_p} g, \tag{6}$$

where the acceleration of gravity (g) assumes the negative value of $-9.81\ \mathrm{m\ s}^{-2}$.

When a generic drop falls in stagnant air, its terminal velocity can be obtained from Equation (6) as follows:

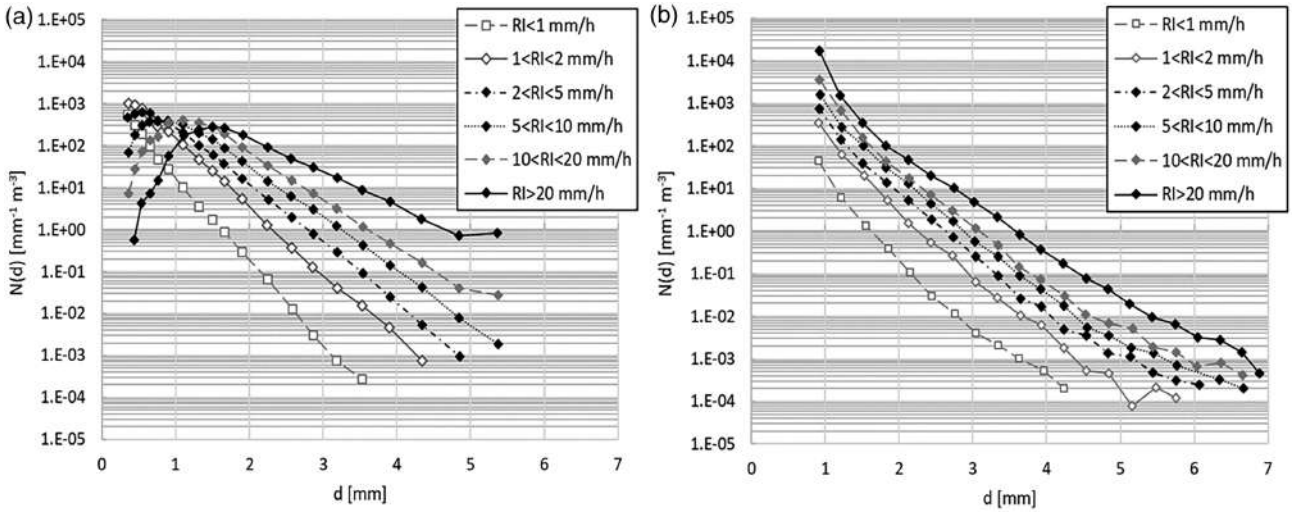

FIGURE 1 Average observed particle size distribution from data collected in Florence (Italy) using a Joss-Waldvogel disdrometer (a) and a Pludix disdrometer (b), for six rainfall rate categories as reported by Caracciolo et al. (2008)

TABLE 1 Parameters a_Y and b_Y of Equation (16), from Rasmussen et al. (1999), for computation of the snowflake terminal velocity w_T, volume V_p, cross-section area A_p and density ρ_p

Crystal type	a_{w_T}	b_{w_T}	a_{V_p}	b_{V_p}	a_{A_p}	b_{A_p}	a_{ρ_p}	b_{ρ_p}
Dry snow	107	0.2	$\pi/6$	3	$\pi/4$	2	0.017	−1
Wet snow	214	0.2	$\pi/6$	3	$\pi/4$	2	0.072	−1

$$w_T = \left[\frac{2V_p\left(\rho_p - \rho_a\right)g}{C_D A_p \rho_a}\right]^{1/2}. \tag{7}$$

The drag coefficient (C_D) is a dimensionless quantity used to represent the resistance of an object in motion in a fluid, such as air or water, and is associated with the cross-sectional area of the object (A_p). The estimation of the drag coefficient is not easy. In the literature, various experiments were carried out with the objective to identify a relationship between the drag coefficient and the particle dimension and/or its terminal velocity for hydrometeors falling through the atmosphere (see e.g. Beard, 1976; Gunn & Kinzer, 1949).

In the work of Rasmussen et al. (1999) observed data from the Marshall Snowfall Test Site, near Boulder (Colorado), of the National Center for Atmospheric Research, were classified into a large number of crystal types (e.g. dendrites, hexagonal plates, lump graupels, etc.) and aggregated into two macro categories: 'dry' and 'wet' snow. In that work, the volume V_p, the cross-section area A_p, density ρ_p and terminal velocity w_T of each type of snowflake are parametrized with a power law curve as a function of the equivalent particle diameter d:

$$Y(d) = a_Y\, d^{b_Y}, \tag{8}$$

where Y assumes the nomenclature of the volume V_p, the cross-section area A_p, density ρ_p and terminal velocity w_T, while a_Y and b_Y are the parameters associated with each type of snowflake.

In Table 1, as an example, the values of the power law parameters for dry and wet snow provided by Rasmussen et al. (1999) are reported. When the particle diameter is expressed in centimetres, the following parameters provide w_T in m s^{-1}, V_p in cm^3, A_p in cm^2, and ρ_p in g cm^{-3}.

2.3 | Drop shape

Some measurement principles exploited by non-catching type gauges detect the dimension of the horizontal axis of the drop to calculate its volume. Small drops, up to 1 mm diameter, are almost perfectly spherical. Larger drops are flattened by the dynamical pressure applied by the air. Different theories exist to model the shape of the drops as a function of their equivalent diameter (diameter of a sphere with an equal volume). The result of one of these theories is presented in Figure 2 (from Beard & Chuang, 1987). The drop

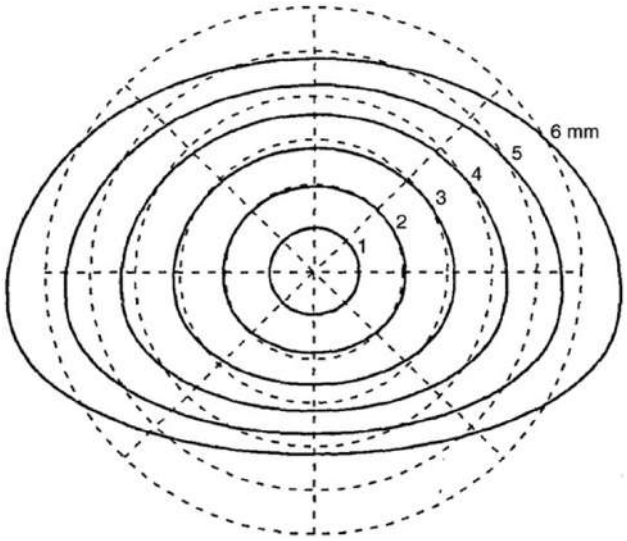

FIGURE 2 Shape of falling drops as a function of their equivalent diameter.
Source: Beard and Chuang (1987)

surface can be represented by following the equation developed by Pruppacher and Pitter (1971) as a function of the equivalent radius a_o, the deformation coefficient c_n and the polar angle from the forward stagnation point θ. The c_n values are listed in the two mentioned works as a function of drop size.

$$\mathrm{r} = a_o(1 - c_n \cos(\theta n)). \tag{9}$$

Some theories, such as the model of Pruppacher and Pitter (1971), predict a recurved base (a small dent present at the base of the drop) for large drops. Further to this equilibrium shape, vibrations appear in falling drops. These oscillations are typically at a frequency of a few tens of Hz or an oscillation period of a few tens of milliseconds (Szakall et al., 2009).

The balance among the forces of surface tension, hydrostatic pressure and aerodynamic pressure from airflow around the drop determines the shape and the terminal fall velocity of hydrometeors. Green (1975), using a simple hydrostatic model, represented raindrops as oblate spheroids with axis ratios determined by the balance of surface tension and hydrostatic forces. Pruppacher and Beard (1970), by means of wind tunnel experiments, found that the raindrop shape can be defined in terms of the axial ratio (b/a) between the vertical (b) and the horizontal axis (a). For raindrops with equivolumetric drop diameter d between 1 mm and 9 mm, they obtained the following empirical equation:

$$\frac{b}{a} = 1.03 - 0.062\, d, \tag{10}$$

while for $d < 1$ mm the axial ratio is $b/a = 1$.

Beard and Chuang (1987) introduced the contribution of the aerodynamic pressure in equilibrium condition, and provided a model to explain the drop shape with its characteristic flattened base that increases with drop size and, for drops having a diameter between 2 and 6 mm, can be expressed in terms of the following polynomial:

$$\frac{b}{a} = 1.0048 + 5.7\,10^{-4}\, d - 2.628\,10^{-2} d^2 + 3.682\,10^{-3} d^3 - 1.677\,10^{-4} d^4. \tag{11}$$

Model results of Beard and Chuang (1987) were consistent with the experiments of Chandrasekar et al. (1988) and Bringi et al. (1998), who employed aircrafts to study the shape of raindrops in natural rainfall.

3 | NON-CATCHING PRECIPITATION GAUGES

The initial manual measurement methods for the study of the hydrometeor's characteristics evolved due to advances in technology and electronics. Nowadays, different techniques are involved in the determination of liquid/solid particle characteristics, like devices to measure the displacement and mechanical energy caused by raindrops/graupels hitting a surface, optical imaging to measure the velocity, diameter and shape of the drops hitting a diaphragm and optical detection, whereby the size, shape, velocity and diameter of hydrometeors are measured while they cross a light or laser beam, and so forth.

3.1 | Optical gauges

Optical disdrometers use visible or infrared (IR) light to detect hydrometeors. They are equipped with IR or visible light transmitters that illuminate a volume of the atmosphere and use optical sensors to detect the light emitted from the transmitter. The illuminated measuring volume is usually defined by the shape of the lens and the relative position between the transmitter and the receiver. When hydrometeors cross the sensing volume, the light changes its intensity and scatters in various directions. This variation is detected by the sensor allowing the physical properties of the particle (e.g. the diameter and the fall speed) to be derived. A simple schematic of the optical principle and configuration is shown in Figure 3.

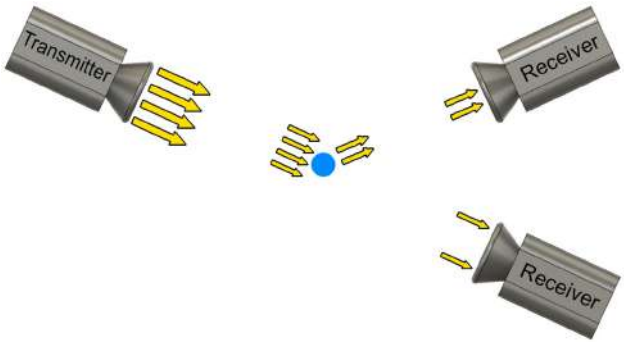

FIGURE 3 Schematic of the optical principle and configuration

Three physical configurations for optical gauges are commonly adopted. In the first case, here called *optical transmission*, the receiver is in front of the transmitter and captures the direct beam of light so that, when hydrometeors intersect the beam, light is partially scattered and its intensity at the receiver is lower. In the second case, here called *optical scattering*, the receiver is not located in front of the transmitter but at a given angle. In the absence of any obstruction, the signal at the receiver is very low, whereas when hydrometeors cross the measurement volume the light is scattered in various directions including the one of the receiver, therefore increasing the signal amplitude. The last type of instruments is based on *optical imaging* technology, where the instrument captures images of the passing hydrometeors that can be further processed to obtain their physical properties.

3.1.1 | Optical transmission

Instruments based on optical transmission are composed of a light source (typically an IR light emitting diode, IR-LED), which produces a homogeneous light beam, and a receiver (typically a photodiode). The light sheet has a width of a few cm, a length of a few tens of cm and a thickness on the order of 1 mm, resulting in an analysed volume of a few cm^3. When no hydrometeors are present within the measuring volume, the intensity of the light measured by the receiver is the maximum admissible one and corresponds to the reference level. When a raindrop or ice particle crosses the analysed volume, it casts a shadow over the detector, and the measured voltage is reduced. The amplitude of the voltage drop is proportional to the surface of the shadow, while the duration of the shadow depends on the velocity of the falling particle. Based on such information, the sensor derives the fall velocity and the size of each hydrometeor. The measured particles are classified by the sensor in various predefined classes by coupling the particle fall velocity with their expected diameter. Measurements are flagged and discarded by the instruments if the measured fall velocity of the hydrometeor is far from the theoretical value expected for the measured diameter. This fact can occur when what is measured is not precipitation but an insect, leaf and so forth. From these measurements, the PSD is also calculated. The precipitation rate is derived by integrating over a short interval (typically on the order of 1 min). When measurements are integrated over larger intervals, the total amount of precipitation can be calculated.

An optical disdrometer prototype detecting particles in diameter ranging from 0.3 to 30 mm with velocities up to 20 m s^{-1} is presented by Löffler-Mang and Joss (2000).

3.1.2 | Optical scattering

When light encounters a hydrometeor, part of the intensity is scattered in various directions, depending on the wavelength of the emitted light and the size of the drop. For IR light and typical drop sizes (0.1–6 mm), the angle of maximum diffraction is around 45°. This principle is used by optical scattering instruments (Figure 4) to detect hydrometeors in the atmosphere and derive the associated precipitation rate. A light source (typically IR-LED) emits a cone of light. A photodetector is placed at an angle of 45° with the source. The intersection of the light source and the cone of vision of the photodetector defines the analysed volume (typically, a few hundreds of cm^3). Instead of a cone of light, the source can also be a light sheet to decrease the analysed volume (down to a few cm^3) and increase the resolution. Because the scattered intensity is low, it is important to use a source with a sharp bandwidth and a filter in front of the detector to measure only the wavelengths emitted by the source. A lock-in can also be used to increase the accuracy, with a light source being modulated at a certain frequency, and the electrical signal being analysed at that frequency.

In undisturbed conditions, when no particles occupy the analysed volume, the signal measured by the photodetector is very low because the direction of the light differs from that of its cone of vision. When a particle travels through the measuring volume, the light is scattered in different directions and is partly detected by the photodetector, which records a peak in the signal. From the characteristic frequency of the emitted signal, the returned signal is filtered to obtain only the components related to the falling hydrometeors. The small particles in suspension induce a base level of this characteristic frequency that can be linked to the visibility. Each time a

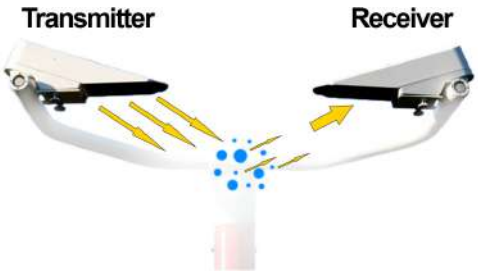

FIGURE 4 Scheme of an optical scattering sensor and measuring principle

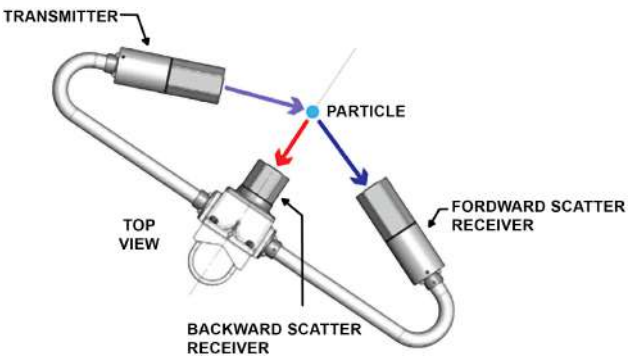

FIGURE 5 Schematic of the optical sensor with two receivers to detect the forward and backward scatter
Source: Biral Ltd., brochure on visibility and present weather sensor for aviation

raindrop falls in the analysed volume, a peak is observed. The amplitude of the peak is proportional to the drop size, hence it is possible to obtain the PSD, therefore the total precipitation and precipitation rate.

Recently developed instruments are equipped with two receivers, one that measures the forward scatter and the second one, usually positioned as shown in Figure 5, which receives the backward scatter. One of the detectors identifies the forward scatter radiation and it is usually located between 39° and 51°, meanwhile the other detector identifies the backward scattered radiation (107°–119°). The second receiver improves considerably the performance of these instruments because it allows to discriminate between liquid and solid precipitation by combining the two signals. The ratio between the back and forward scattered signals allows to estimate visibility and to discriminate between different types of precipitation. Indeed, snow and other frozen hydrometeors have a much higher proportion of back scattered light when compared with rain.

3.1.3 | Optical imaging

These gauges use a charge-coupled device (CCD) or complementary metal–oxide–semiconductor (CMOS) photographic sensor, operating in the visible band of the light spectrum, to capture an image of each single hydrometeor that crosses the sensing volume. Two different types of sensors can be used, line-scan and total image sensors. The first is composed of a single line of pixels that can be read at high frequency; the image is therefore obtained after pre-processing and assembling the consecutive slices. These kinds of sensors are commonly used in the industry for high-speed machine vision operations and can reach very high spatial and temporal resolutions. Total image sensors are instead composed of a 2D array of pixels and capture still pictures of the hydrometeors, the data obtained are directly usable without pre-processing but usually have lower spatial and temporal resolution.

The line-scan camera is employed for example by the 2D video disdrometer (2DVD) (Figure 6, left), manufactured by Joanneum Research at The Institute for Applied Systems Technology in Graz, Austria. Inside the gauge, a visible light source generates a light sheet that is projected onto a line-scan camera, as shown in Figure 6 (right panel). The 2DVD uses two orthogonal light sheets and two synchronized cameras. The light sheets are quite bright and particles falling through them cast shadows on the photodetectors. The resulting signals are compared against a threshold to determine if a pixel is lit or obscured. The combination of bright light and video thresholding renders the raindrops opaque and makes the 2DVD insensitive to ambient light.

The two orthogonal projections provide, in principle, 3D raindrop shape information and can limit the shadowing effect that can happen when two hydrometeors cross the beam exactly at the same time. Shape information allows computation of the drop volume and equivalent drop diameter, as well as the oblateness. The light sheets are spaced 6.2 mm apart and the 2DVD software matches particle shadows in the upper light sheet with particle shadows in the lower sheet. By measuring the time needed for a particle to move 6.2 mm vertically, it is possible to obtain its vertical velocity. The 512 photodetectors are read out at a rate $f = 34.1$ kHz, creating slices of the image projection, and with this information it is possible to reconstruct the shape of the hydrometeor using the same principle of a flatbed scanner.

Another optical imaging gauge is the high-speed optical disdrometer (HOD), illustrated in Figure 7. In this case, however, the instrument uses a total image sensor. The main components of the HOD are a high-speed CCD camera, an LED light with a diffuser and a digital fibre-optic sensing unit. The camera and the light are

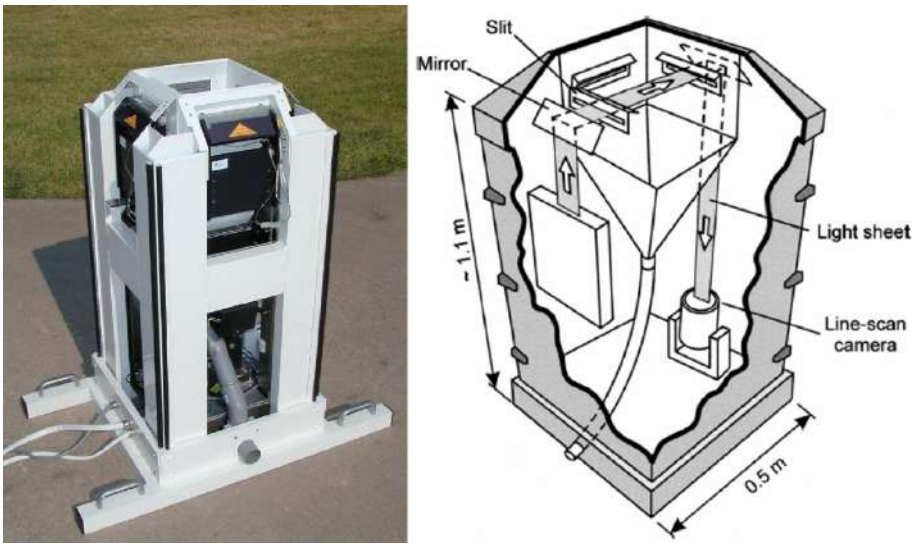

FIGURE 6 Image of the 2D video disdrometer (left panel – Photo from S. Fredrickson, website of the NOAA National Severe Storms Laboratory) and measuring principle scheme (right panel – Source: Kruger & Krajewski, 2002)

FIGURE 7 Image of the high-speed optical disdrometer
Source: Testik and Rahman (2016)

installed at a distance of 160 cm, and the sensor is installed between the camera and the light source, with the camera focal plane centred 60 cm away from the camera. The sensor installed in the HOD captures raindrop images at 1000 frames per second with a resolution of 1024 × 1024 pixels. The measurement volume is defined by the vertical size of the camera view frame (70 mm) and the horizontal sensing area, which is defined by the sensor beam width (5.25 mm centred around the focal plane) and the transverse size of the camera view frame (70 mm). This configuration corresponds to a measurement volume of 25.73 cm^3. The images are recorded only when there is a raindrop within the measurement volume by utilizing a -sensor-based camera triggering system.

3.2 | Impact disdrometers

These instruments exploit the kinetic energy of the falling drops when impacting the exposed surface of the gauge. A plastic or metal membrane is used at the measurement surface to sense the impact of single precipitation particles. In some systems, the mechanical movement of the membrane is transduced into an electrical signal by an attached moving magnet/coil system. In other solutions, the amplitude and the frequency spectrum of vibrations generated by precipitation particles hitting the membrane are detected and analysed to determine the particles size and numerosity. Impact methods are therewith suitable to determine the particle frequency (drops s^{-1} m^{-1}), the rain rate (mm h^{-1}) and the drop size distribution over a given time window.

Impact disdrometers can be divided into two categories: acoustic disdrometers and displacement disdrometers. Both types are commercially available. Both acoustic and displacement disdrometers are devoted to measure liquid precipitation, because the energy of the drops is directly related to the mass and density of the water drops; snowflakes and hailstones, for example, have completely different impacts on the sensor surface, and may lead to underestimation or overestimation of the precipitation measures.

3.2.1 | Electro-acoustic devices

In electro-acoustic devices, the falling precipitation particles (raindrops or graupels) impact a target or sensor cover made of metal or plastic (Figure 8). The amplitude of the pulse produced by the impact is a function of the vertical momentum of the particle and thus of its mass and terminal velocity. The pulse can be detected either by an electrical force transducer, for example, piezoelectric (Förster et al., 2004; Salmi et al., 2005, 2011),

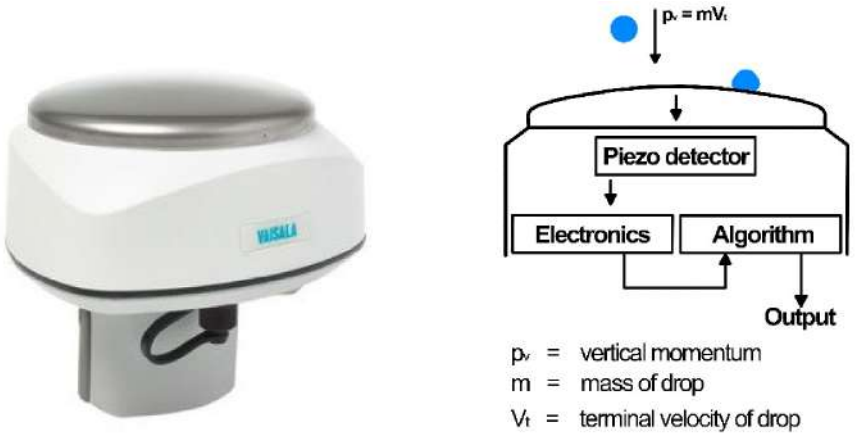

FIGURE 8 Image of the Vaisala electro-acoustic impact disdrometer and its functioning scheme
Source: Salmi et al. (2005)

mechanically attached or linked to the sensor cover, or transmitted through a media to a microphone (Kinnel, 1972). The electrical transducer produces an output voltage that is a measure of the impact force (change of momentum over time) and thus the volume of the drop and the impact duration, which is the impact velocity. Knowing the area of the sensor cover and the time window, the rain rate and the accumulated precipitation can be calculated. To distinguish between raindrops and graupels, the characteristics of the waveform can be used, as ice and water produce very different waveforms. With assumptions on the hydrometeor velocity and density, its kinetic energy may be derived (Löffler-Mang et al., 2011).

3.2.2 | Displacement devices

In displacement disdrometers, the sensor cover is displaced when impacted by the falling precipitation particle. The displacement impact disdrometer was presented in Joss and Waldvogel (1967). A magnet, moving in a coil, is mechanically attached to the cover and translates via magnetic induction the energy generated by the impact to an electrical pulse (voltage), as shown in Figure 9. Analogous to the electro-acoustic devices, the electrical signal is a measure of the impact force, which is used to calculate the volume of the drop and the principle for determining the rain rate, and the accumulated precipitation, is similar. As the instrument contains moveable parts, it may require regular maintenance.

3.3 | Radar instruments

In situ precipitation measurement instruments employing microwave sensors, also called microwave or radar disdrometers, are low-power, small-size Doppler radars, vertically looking (without scanning capabilities) that exploit the Doppler effect due to falling drops to derive the spectrum of precipitating particle size. Continuous wave (CW) radars use different antennas to transmit and receive the microwave signal, while frequency-modulated continuous-wave (FMCW) radars are also available and able to measure height-resolved drop size distributions (Löffler-Mang et al., 1999).

Radar disdrometers operate by measuring the power of the backscattered signal and its Doppler shift to estimate the size of hydrometeors passing nearby, as described by Sheppard (1990) and Prodi et al. (2000). A falling drop, moving vertically towards the instrument, produces a return signal when entering the measurement volume. The return power (P_r) can be expressed as follows (Sheppard, 1990):

$$P_r = \frac{P_t \cdot L_w \cdot G_t(R1) \cdot G_r(R2) \cdot \lambda^2 \cdot \sigma}{64\pi^3 |R1|^2 |R2|^2}, \tag{12}$$

where P_t is the transmitted power, L_w is the transmission loss due to the wetting of the radomes, $R1$ and $R2$ are the distances between the emitting antenna and the falling drop, and between the drop and the receiving antenna, respectively (Figure 10), $G_t(R1)$and $G_r(R2)$ are the antennas' respective gains, λ is the emitted frequency and σ is the scattering cross-section.

The Doppler shift (f_d) is a function of the velocity vector ($\mathbf{v}$) of the object when crossing the equi-phase surfaces having $R1 + R2 =$ constant (Figure 10), and can be obtained using Equation (13), as a function of the phase shift gradient ($\nabla\varphi$) with the phase shift (φ) calculated from Equation (14).

$$f_d = \nabla\varphi \cdot \frac{\mathbf{v}}{2\pi}, \tag{13}$$

FIGURE 9 Image of the Joss-Waldvogel displacement impact disdrometer and its functioning scheme.
Source: Kathiravelu et al. (2016)

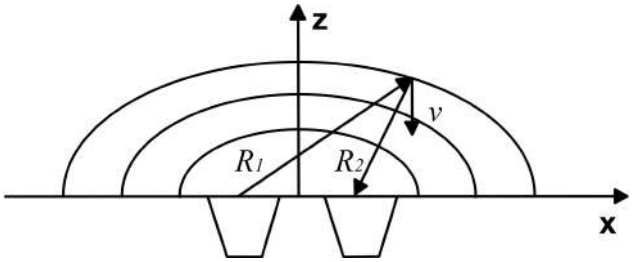

FIGURE 10 Configuration of the emitting (left) and receiving (right) antennas
Source: Prodi et al. (2000)

$$\varphi = 2\pi \frac{|R1| + |R2|}{\lambda}. \tag{14}$$

For a single drop, the return power depends on the backscattered signal that is a function of the scattering cross-section σ and the drop diameter. From measurements of the return power alone, depending on the instrument operating frequency, it may not be possible to uniquely determine the hydrometeor diameter because of Mie scattering that can occur for larger drops (Rauber & Nesbitt, 2018). The phase shift, on the other hand, is a function of the particle velocity, which is directly related to its diameter if the drop falls at terminal velocity. Semi-empirical relationships are used for rain and for different frozen hydrometeors (hail and snow). For raindrops, for example, Atlas et al. (1973) derived the following relationship:

$$v(d) = 9.65 - 10.3e^{-0.6d}, \tag{15}$$

where d is in mm and v is in m s^{-1}. During a precipitation event, the return signal is composed of the sum of the contribution of each drop and is usually collected in 1-min segments, which are then processed using Fourier transform to evaluate their spectrum. For the signal analysis, natural rain is considered as a superposition of monodisperse events, so that the spectral intensity of the return signal, $S(f)$, is as follows:

$$S(f) = \int_{d_{min}}^{d_{max}} N(d)V(d)\bar{S}(d,f)\mathrm{d}d, \tag{16}$$

where $\bar{S}(d,f)$ is the volume-averaged Doppler power density and $V(d)$ is the measuring volume. The number of drops in the measurement volume can be obtained once the value of $\bar{S}(d,f)$ is known, at least in a discrete form. Evaluation of $\bar{S}(d,f)$ can be achieved using laboratory measurements of monodisperse drops (Prodi et al., 2000) or from numerical simulation once all the antennas' parameters are known. A more in-depth and detailed explanation can be found in the work of Sheppard (1996).

Different models of microwave disdrometers have been developed (Figure 11), but the measuring principle of this kind of gauges remains unchanged. During field intercomparison and testing, multiple instruments were compared against other disdrometers (optical or impact) and more traditional catching-type gauges, showing sufficient agreement on the cumulated event precipitation but low agreement on RI, especially for heavy precipitation events and measurements at 1-min time resolution (Caracciolo et al., 2006; Prodi et al., 2000; Vuerich et al., 2009).

One limitation of this instrument is that the terminal velocity of the falling drops is calculated using a model that does not consider the presence of wind. Due to the position near the ground of these instruments, it is acceptable to assume that the vertical component of wind is negligible, but it still has to be investigated the effect of the horizontal component of wind on radar measurements (Caracciolo et al., 2006). Because the Doppler shift depends on the hydrometeor velocity component in the direction of the antennas, a horizontal component of velocity can modify the Doppler shift and consequently

FIGURE 11 Microwave precipitation gauges: LCR PVK ATTEX on the left (from Cauteruccio et al., 2021a) and Pludix on the right (from Caracciolo et al., 2006)

the instrument assumption on the diameter. This problem is usually limited by the manufacturer by shaping the antennas' emission into a narrow cone. Another critical aspect is related to the evaluation of $S\overline{c}(d, f)$ if it is obtained by laboratory calibration. In this case, it is imperative that all the released drops achieve terminal velocity before entering the sensing volume, because an accelerating drop generates a backscattered signal that differs both in frequency and amplitude from the one generated by a drop falling at terminal velocity.

4 | EXISTING CALIBRATION PROCEDURES

Information about the calibration procedure adopted by manufacturers are usually undisclosed, but in some cases, like Vaisala (Tuukka, 2015), the calibration procedure is described, at least in a simplified form. In the Vaisala calibration laboratory, they developed a rainfall generator (Figure 12, right) that can be positioned above the instrument. A 'dripper tank' (Figure 12, left) is raised 14 m over the instrument and drops of fixed diameter are released continuously onto a screen just under the tank. The idea is that the constant size drops after hitting the grid are broken into smaller drops of random size that would reproduce a realistic precipitation event.

Just above the gauge under test, an optical instrument measures the incoming precipitation and is used as a reference. The precipitation intensity can be varied by increasing or decreasing the flow to the 'dripper tank' and different PSD are generated by changing the distance between the tank and the redistribution screen. The optical reference is composed of two laser emitters that produce two different sheets of light and two sensors that measure the received intensity. Assuming that only one drop crosses the light beam at the same time, the drop dimension is obtained by the reduction in the laser beam intensity while the time that the particle needs to cross both sheets is used to calculate velocity.

Finally, all the released drops are collected under the instrument and a weight scale is used to obtain the cumulated water amount. This approach has the advantage of producing drops that fall almost at terminal velocity. On the other hand, because of the method used for generating drops, it is not possible to freely choose the drop crossing position with respect to the sensing area, which would allow, for example, to assess the effect of the non-uniformity of the beam for laser precipitation gauges. Also, the physical principle used for checking the generated drop in flight is very similar to that used by some of the instruments that could be calibrated and presents the same limitations and shortcomings, being not the ideal reference for calibration purposes.

The calibration procedure used by the manufacturer is known also for the Thies LPM (Thies-Clima, 2011; Lanzinger et al., 2006), another optical disdrometer. The factory calibration comprises the determination of the geometrical shape and size of the laser light sheet and a calibration of the drop volume measurement. The characteristics of the light sheet such as beam width and alignment are exactly measured by using an optical beam analyser. For the volume calibration, an automated calibration bench is used. It consists of a precision dispensing pump with an accuracy of 0.3% and a drop generator that is mounted on a 2D positioning system. Uniform drops with a diameter of about 3 mm are released through the light sheet at 15 equally distributed positions. At each position, 30 drops are released. Based on the repeatability of the disdrometer measurements at any fixed position,

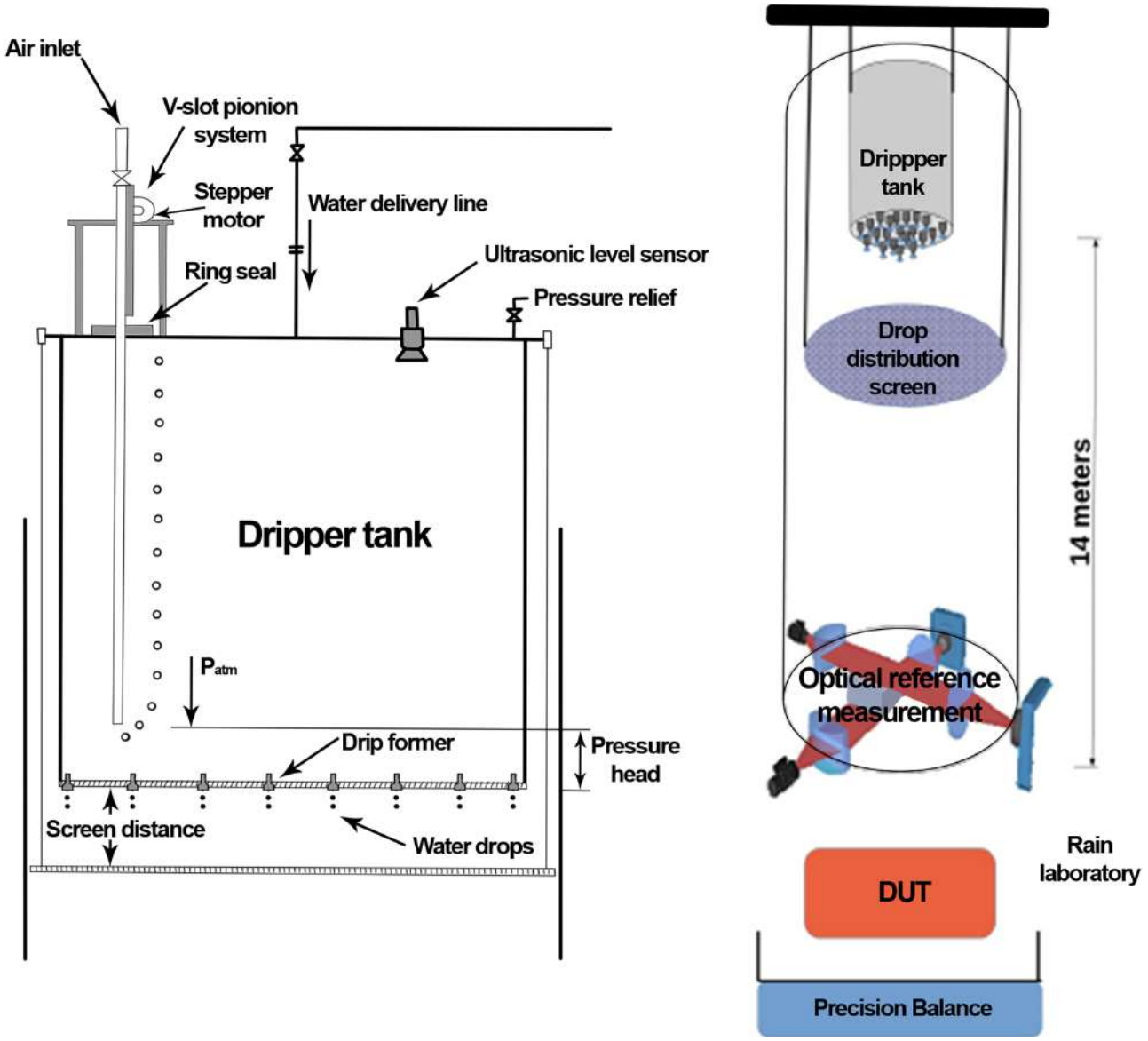

FIGURE 12 Schematics of the Vaisala calibration tower (Source: Tuukka, 2015) with the 'dripper tank' as a drop generator (left panel) and a sketch of the whole setup (right panel), where DUT indicates the disdrometer under test

the uniformity of the drop diameters can be estimated to 2%. The calibration process is carried out in two steps allowing to assess the deviation of the mean volume from the reference. After the first run, the device is adjusted by setting appropriate calibration parameters. In a second run, the adjustment is checked. The manufacturer obtained a maximum allowed tolerance of 2.2%. This is the estimation of the uncertainty for the volume measurements under laboratory conditions provided that a large number of drops fall in equally distributed positions through the light sheet. It does not apply to the volume measurement of a single drop. This procedure is based on the specific characteristics of the targeted instrument and allows controlling the position of each released drop. However, the drop diameter and velocity are not preliminarily measured, independently on the instrument under tests, therefore no reference is actually available, and it is unclear if drops are released from a sufficiently high elevation to approach terminal velocity. Finally, only one drop diameter is investigated, so that significant errors could arise when different drop diameters are measured.

When information about the manufacturer calibration is not available, the only source of information is the scientific literature. For example, in the work of de Moraes Frasson et al. (2011) another approach for calibrating the Thies LPM is proposed. In their procedure, the diameter of a calibrated metallic sphere is repeatedly measured by the disdrometer and then contrasted to its

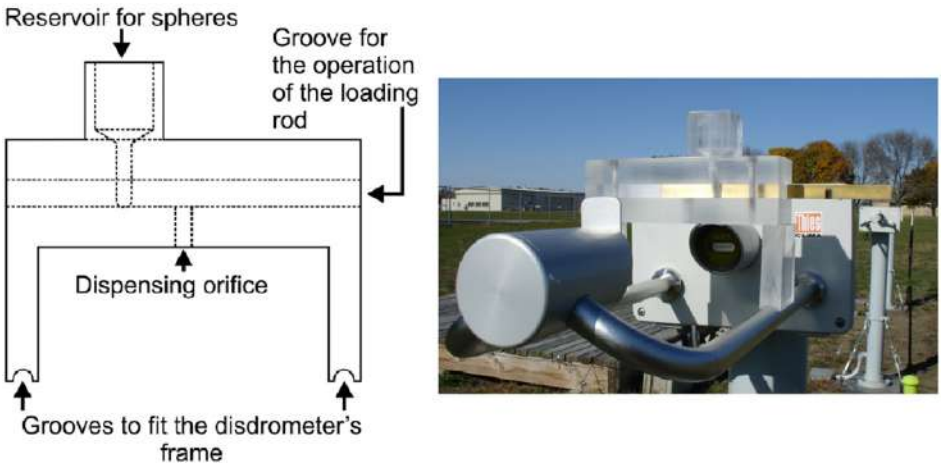

FIGURE 13 Calibration apparatus scheme (left panel) and operational use (right panel) for the Thies LPM disdrometer
Source: de Moraes Frasson et al. (2011)

nominal diameter. They developed a device to deploy metallic spheres of 2, 3, 4, 5 and 6 mm in diameter on approximately the same position of the disdrometer's laser sheet (Figure 13). The device consists of a reservoir for the spheres, ending in a tunnel that leads them to the loading rod. The loading rod has a set of grooves, each one matching the size of the sphere currently being used. When the groove is aligned to the reservoir, it allows one sphere to be loaded. The loaded sphere is deployed when the loading rod is moved to the releasing position and the loaded groove is aligned with an opening at the bottom of the calibration device. The calibration device has two supports that adjust to the disdrometer's frame and align the centre of the device's outlet with the centre of the laser beam. The release height of the spheres is chosen to provide the spheres with enough height to achieve a velocity of approximately 1 m s^{-1} at the height of the beam. The steel spheres had their diameter checked with a calliper, and the authors found no deviations from their nominal diameter to a tenth of a millimetre. For this reason, they assumed that the nominal diameter is the real diameter of the sphere, which allowed them to refer to the difference between disdrometer measurement and nominal diameter as a measurement error. The average error for each instrument is an indication of the bias in the diameter measurement, while the standard deviation of the error will characterize the uncertainty of the diameter measurement. This procedure is extremely simple, but the use of metallic spheres is only compatible with some types of non-catching gauges, like the optical ones. Also, the fall velocity of the spheres is not considered, meaning that only one of the two parameters measured by disdrometers can be calibrated.

In the work of Testik and Rahman (2016), different laboratory experiments were designed to evaluate the measurement accuracy of the HOD and its performance in a controlled environment. The laboratory tests involved experiments with high-precision spherical calibration lenses and free-falling water drops of known size. In the first set of laboratory tests, spherical lenses with diameters of 0.5, 1, 3 and 5 mm with a diameter tolerance of 62.5 μm were adopted. Spherical lenses were made of two different materials, fused silica and sapphire, with refractive indices of 1.46 and 1.77, respectively. These tests provided information on the overall measurement errors, including both hardware- and software-related errors, and within the simplified hypothesis of spherical object. Results showed that the maximum percentage error in the measurement of the diameter decreases with increasing the diameter and the maximum deviation is about 11% for the sphere with a diameter of 0.5 mm. The second set of laboratory tests was carried out with free-falling water drops of various sizes generated using needles attached to a constant-head tank as shown in Figure 14. The constant-head tank was used while fixing the needle to generate drops of nearly the same size throughout the test. The average equivalent drop diameter was derived based on the total volume released in each test. Larger drops, compared with the spherical lens, were released with diameter between 2.0 and 5.0 mm. Water drops were released at 60 cm above the measurement volume. Each released drop triggers the HOD and 10 images of the same water drop are captured. The error in the measurement was derived and expressed in terms of total volume; the generated water drops were collected in a graduated cylinder, and the total volume of the collected water was measured and compared with the total volume of the drops measured by the HOD. The measure of the total volume within the graduated cylinder is affected by an error of about 0.5 mL. These tests provided a maximum percentage error in HOD measurements of 9.2% in terms of water volume. This procedure is similar to the previous one and presents similar shortcomings both in terms of the

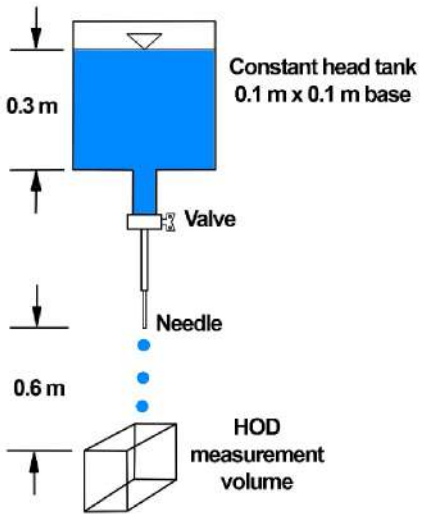

FIGURE 14 Scheme of the laboratory setup used to calibrate the high-speed optical disdrometer (HOD)
Source: Testik and Rahman (2016)

lack of a reference measure for drops diameter and velocity and because it has limited applicability to some types of instruments only.

From the work of Licznar et al. (2008), information is obtained about the calibration procedure of impact disdrometers called "DBI impactometers", developed at the Department of Building and Infrastructure (DBI) of the Wroclaw University of Environmental and Life Sciences, as used by the Institute of Fundamental Technological Research of the Polish Academy of Sciences (IPPT PAN). The instrument output was recorded for several single water drops with various known volumes and fall velocities. The drops were free-falling in still air conditions after being released at different elevations. Their velocities just before the impact were measured using a high-speed digital video camera (Figure 15), at 25 cm above the sensing plate of the DBI impactometer. The interval between the camera frames was set to 0.8 ms, and the exposure time was set to 0.2 ms. The waterdrops were generated through a thin silicon pipe (adapted from a medical intravenous infuser kit manufactured by Polfa Lublin SA) ending with the medical needle of selected diameter. The different diameters of the needles controlled the waterdrop size. An Ascor syringe pump, type 'Ap 12', was used to supply distilled water to the pipe at a constant rate. The regulated outflow rate of the pump controlled the frequency of waterdrop release. The diameter of the falling drops was measured directly from the pictures taken by the camera with fixed setting. As a reference, a picture of a square-grid paper sheet (with a grid size of 1 mm × 1 mm), placed along the falling route of the waterdrops, was used. The reference-grid picture was taken at the same camera setting as for the rest of the experiment. As an independent verification of the drop diameters, they were also weighted with accurate laboratory scales. The DBI impactometer was tested for single drops falling from three different elevations: 2.34, 11.68 and 26.00 m. Tests for the 2.34 m falling height were conducted in the laboratory room in steady air conditions. The test runs for the two other elevations were performed in the interior staircase of the IPPT PAN building. The air temperature measurements made on different floors showed only small variations from 21.0 to 22.3°C, while the airflow velocities were below 0.08 m s^{-1}. Preliminary tests of the DBI impactometer revealed that its output depends not only on the waterdrop diameter and impact velocity but also on the distance between the drop landing position and the centre of the sensing plate. This procedure is capable of producing drops of various size falling at their terminal velocity, and employs an independent measure of both drops diameter and velocity. One limitation is the cost of high-resolution high-speed video cameras and the lack of an automated procedure to be used to calibrate a large number of instruments.

Another calibration procedure found in the literature for impact disdrometer is based on the numerical minimization of a function, similar in philosophy to an adaptive digital filter. The strategy behind this technique is to use a tipping bucket rain gauge or another reference gauge to provide the data to optimize a set of adaptive coefficients. An error surface is defined as the sum of the square of the differences between the disdrometer cumulated volume and the reference cumulated volume. The calibration function is obtained with a series of iterative steps in which the coefficients are obtained by minimizing the error surface (Kourtellis et al., 2005).

This approach is based on real precipitation events, meaning that it is influenced by the environmental conditions at the test location, and requires a large amount of time to calibrate each instrument. The most important drawback is the use of a tipping bucket rain gauge, which measures neither the diameter nor the velocity of hydrometeors, and its adoption as a reference for the calibration of a disdrometer is rather questionable.

To assess the performance of impact disdrometers in measuring hail, a peculiar calibration method has been recently proposed by Löffler-Mang et al. (2011). The hail precipitation event was reproduced in laboratory using a hail gun, specifically designed, and spheres made of ice or frozen fruit juice, to resemble more spongy ice.

After thoroughly searching the scientific literature, the most recurring idea for testing the performance or calibrating disdrometers seems that of using plastic or metal

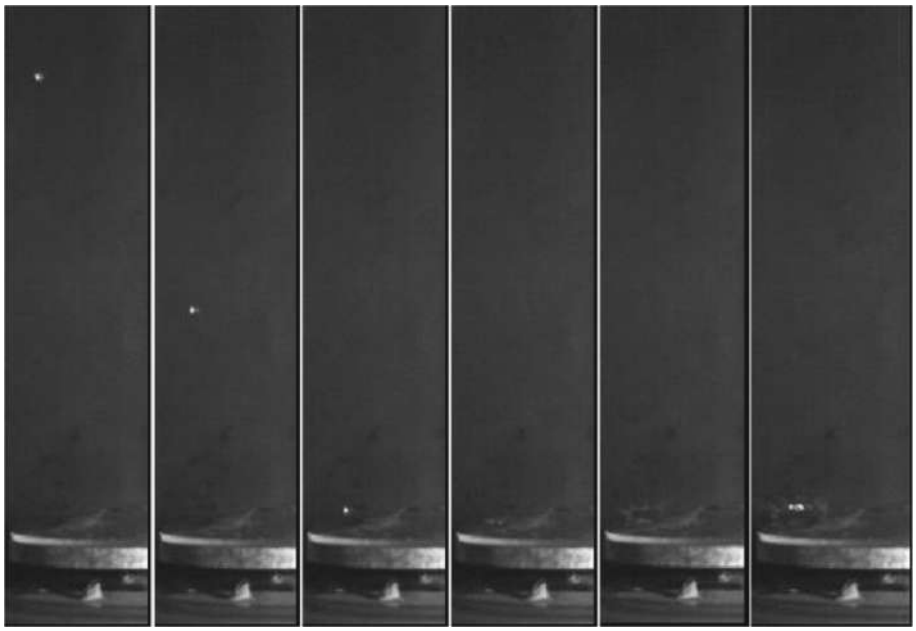

FIGURE 15 Images captured by the high-speed camera used to estimate the drop velocity just before the impact. *Source:* Licznar et al. (2008)

FIGURE 16 Image of the Styrofoam particles used by Bernauer et al. (2015) to simulate solid precipitation

spheres of a known diameter, released over the sensing area of the instrument. This solution is adopted because of its simplicity and repeatability, and examples of this method can be found in Grossklaus et al. (1998), Löffler-Mang et al. (2011) and Kruger and Krajewski (2002). In one case, following the same basic idea, small pieces of Styrofoam (Figure 16) were used, instead of spheres, to better simulate snowflakes (Bernauer et al., 2015). The use of water drops is limited and in most cases only drops of relatively large diameters are used. As discussed before, the use of solid media as a substitute for water drops is less than ideal and should be avoided, because it can reproduce neither the peculiar shape of falling drops nor their terminal velocity.

5 | INFLUENCE OF PARAMETERS

5.1 | Wind

Wind is recognized as the major environmental source of precipitation measurement errors. The effect of wind on precipitation measurement is also called the *exposure effect* in the literature (since Jevons, 1861). The gauge body, immersed in a wind field, behaves like a bluff-body obstacle in the free flow, and produces strong velocity gradients, upwards or downwards components and turbulence close to the gauge (Cauteruccio et al., 2020). The hydrometeors trajectories are diverted by the velocity field around the instrument (Cauteruccio et al., 2021a; Cauteruccio et al., 2021b; Cauteruccio et al., 2021c; Colli et al., 2020; Folland, 1988; Jevons, 1861; Nešpor & Sevruk, 1999) and, depending on the gauge shape and wind speed, the number of hydrometeors that cross the sensing volume is affected, leading to an over- or under-estimation of the precipitation intensity. The exposure effect therefore introduces an error, common to all precipitation gauges, that is simply due to the presence of the instrument itself (invasive measurement) and varies with the gauge shape, wind speed and direction, and the PSD.

Wind also changes the velocity of the falling hydrometeors. In fact, particles immersed in a wind field reach a horizontal velocity roughly equal to the wind speed, while vertical components near the instrument, induced by the exposure effect, affect their vertical velocity. For non-catching type gauges, the change in the hydrometeors absolute velocity introduces further potential error because, in most cases, they explicitly use velocity to estimate hydrometeors size and they assume that trajectories are always vertical. Impact gauges, for example, measure the kinetic energy of the drop, which is a function of the drop's absolute velocity, and these instruments usually assume that hydrometeors fall vertically at terminal velocity, completely neglecting the horizontal component, which increases the kinetic energy of the drop. A similar problem is found in radar disdrometers. They measure the Doppler shift, which

depends on the component of velocity in the direction connecting the hydrometeor and the antenna phase centre, therefore the return signal is a function of both the horizontal and vertical velocity components. These instruments assume that the relative velocity is equal to the terminal velocity and then use an empiric relationship to derive the hydrometeor's diameter. It is evident that the presence of wind strongly influences this kind of instruments. To mitigate this problem, manufacturers usually shape the antenna emission into a narrow cone, therefore measuring only the hydrometeors falling near the antenna's axis. Optical instruments in some case can measure the different velocity components (2DVD) or anyhow are less influenced by the horizontal velocity of the drops because they do not explicitly use the velocity to obtain the hydrometeors diameter. Still, the presence of a horizontal velocity component can produce false measurements of particles crossing the sensing volume near the edges. In conclusion, wind affects all precipitation gauges with varying impact on the measurement accuracy, and mitigation actions must be taken, either by the manufacturer (e.g. using aerodynamic shapes and/or software correction) or by the user (e.g. wind shields and/or wind correction curves).

5.2 | Contemporary particle crossings

The contemporary presence of multiple particles in the sensing volume is a further potential source of bias. Most instruments cannot differentiate between multiple hydrometeors that cross the sensing volume at the exact same time and work under the hypothesis that only one drop is present at one time. Optical instruments, except the imaging ones, may interpret simultaneous hydrometeors as one single particle of a larger diameter that is moving faster than a real hydrometeor of the same diameter, potentially resulting in volume overestimation. If the counting algorithm of the instrument discards these measurements, this would instead result in some volume underestimation. Impact disdrometers tend to underestimate the volume of multiple drops impacting the sensor, because they perceive only the effect of the larger drop and neglect the presence of other impacts. This is known as disdrometer dead time issue and may affect measurements during heavy rain events. Optical imaging, radar instruments and in general all instruments that measure an ensemble of hydrometeors at a time do not produce biased measurements in this situation.

5.3 | Drop shape

Most disdrometers work under the assumption that all drops have a spherical shape. This is true for very small hydrometeors but can introduce errors in the measurement of large drops. Optical transmission and scattering gauges obtain the hydrometeor's diameter from the maximum amplitude of the returning signal, which is directly proportional to the maximum diameter of the drop. These kinds of instruments usually assume that the equivalent diameter of the drops is equal to the measured diameter. This hypothesis produces an overestimation of the precipitation volume for oblate hydrometeors, which have a low axis ratio (height/width). The measurement of the fall velocity is also affected since an assumption on the shape of the drop is used in laser disdrometers, where the minor axis dimension is usually set following a pre-determined axis ratio (Battaglia et al., 2010). The drop shape also influences radar disdrometers, which in most cases use a relationship to correlate the signal reflected by hydrometeors into RI that is valid in case of spherical shape. Impact disdrometers are less influenced by the hydrometeor shape because kinetic energy depends only on the hydrometeors mass and velocity but can still influence energy transfer upon impact. All instruments are somewhat affected by this error except those based on optical imaging, where the shape of the drop is one of the measured parameters. In general, however, errors due to the drop shape are limited if compared with other sources of error and corrections can be easily implemented.

5.4 | Further error sources

Most disdrometers show some limitations in their capability to detect the smallest droplets, depending on the specific instrument characteristics and induce a bias in the derived PSD and cumulative precipitation.

Optical disdrometers use a light sheet to illuminate the hydrometeors in the sensing volume. When the drops, especially the larger ones, cross the laser beam near its limits, producing only partial extinction of the beam, an error is introduced that results in some underestimation of the volume. Another source of bias is the uneven power distribution across the beam. This variability means that the amplitude of the return signal depends not only on the hydrometeor diameter but also on its position when crossing the beam. Also, errors in the geometric dimension of the beam can influence the evaluation of precipitation intensity and hydrometeors fall velocity. Another source of error in optical disdrometers is due to spurious drops that can be generated by the breakage of incoming hydrometeors upon impact with the instrument body and can then cross the instrument sensing area.

A typical issue of impact gauges is that the response of the sensor is not constant in the measuring area; it is maximum in the centre and then declines towards the edges,

affecting the accuracy of drop size estimation. Another source of error for impact gauges is due to the drop diameters detection limit. Small drops may not be detected as they cannot be distinguished from ambient noise or because of the 'splash effects' caused by the breakage of large drop. Large drops are also poorly detected because the functional dependency of drop fall velocity to the drop size is very weak for drops larger than 5 mm in diameter, for this reason large hydrometeors are incorrectly classified.

For radar disdrometers, an important source of error is the assumption that the measured Doppler velocity is always equal to the terminal velocity, this is true only if the drop falls along the instrument vertical axis. Instead, the Doppler velocity measured by the instrument is lower and changes with time if the drop falls away from the axis. Other potential sources of error are due to phase stability of the electronics that produce the emitted signal and post-processing, which is required to evaluate precipitation. Because of the complex return signal, the result is highly dependent on the algorithm used and the assumption made in post-processing.

6 | CONCLUSIONS

Manufacturers of meteorological instruments are increasingly developing non-catching type gauges to meet the requirements of National Meteorological and Hydrological Services (NMHSs) and are facing calibration issues due to the nature of the measurand and the highly variable microphysical characteristics of precipitation, even within the same event. Today, each manufacturer implements its own calibration system, either simulating the falling drops with metallic or glass spheres, or other materials, or using simplified raindrop generators.

Traceability of such procedures is still a challenge and the possibility to refer to a standardized procedure based on suitable calibration devices would have a strong impact on the market of non-catching type gauges and in the NMHSs calibration department. Indeed, their diffusion is now limited due to insufficient calibration and any comparison with catching-type gauges highlights their lower performance, showing a significant bias that accurate calibration would possibly eliminate.

Based on the characteristics and limitations of the existing methods, as described in the literature and/or adopted by the manufacturers, the INCIPIT project will develop traceable methods and dedicated facilities for the calibration of non-catching instruments that are used for liquid atmospheric precipitation measurements. The new developments will focus on building up the following instrument testing and calibration chain.

6.1 | Drop generation

The drop generation device must be able to produce a large number of water drops of specified frequency distribution in terms of diameter (volume). When detaching, drops would be about spherical, and a broad range of drop diameters must be possible (indicative from 0.1 to 5 mm), to mimic a sampled particle size distribution (PSD). Initially, a single releasing position will be used, while the generation of a spatial distribution of drops, over a limited surface area (corresponding to the sampling area/volume of the instrument), is desirable. Gravitational methods have been tested already and still need some refinements, while other methods including ejecting drops by using pressure or mechanical moving elements are also possible.

6.2 | Drop acceleration

After detachment, drops will start falling vertically to the ground and accelerating due to the gravitational force (starting from zero velocity if not ejected). Ideally, drops must reach the instrument close to their terminal velocity, which ranges from 1 to 9 m s^{-1}, and would require either introducing a further acceleration or allowing for a sufficient fall height. Since the terminal velocity is achieved asymptotically, a sufficient fraction of its theoretical value could be accepted, for example, 90–95%, which can be obtained with a fall height of few metres. The falling drop also continuously adjusts its shape to compensate the aerodynamic forces acting on the surface, therefore changing from spherical to elongated and assuming the typical hamburger shape (which may lead larger drops to break into smaller drops while falling).

6.3 | Microphysical measurements

Measurement of the microphysical characteristics of the generated precipitation must be performed in the immediate vicinity of the instrument under test to provide the reference quantities for calibration. The main parameters would be the drop size (diameter, volume), vertical velocity and the shape of the drop. It is desirable, although not mandatory, that the measuring principle, used by the calibration system, is different from the one exploited by the instrument under test, and more accurate. Possible methods include laser-based detection and high-speed/high-resolution photography. A complete uncertainty budget must be evaluated for such measurements and traceability ensured.

6.4 | Volumetric and/or gravimetric measurements

Whenever possible, that is when the instrument under test does not deviate the fall trajectory of drops, check of the total amount of water released by the drop generator should be performed by collecting the water and comparing the cumulated amount with the released one. This is especially relevant for the calibration of instruments used to measure precipitation intensity. The whole rainfall generator and the calibration device must be installed in controlled laboratory conditions, while monitoring the influencing environmental variables such as temperature, humidity, pressure and so forth, and avoiding the presence of horizontal air velocity in the testing chamber (which might induce drift in the fall trajectory of drops).

The traceable calibration chain will allow manufacturers to certify the performance of their own non-catching type instruments based on standard procedures. This would allow a much wider penetration on the market, especially responding to the needs of NMHSs for reduced maintenance and fully automated weather stations, thanks to the demonstrated advantages over more traditional catching-type instruments. The lack of accurate calibration and standard calibration procedures is indeed, at present, one of the main reasons why non-catching type instruments are not yet competitive enough to overcome the use of traditional gauges.

It is expected, indeed, that non-contact systems will slowly replace instruments based on the direct interaction between the sensor and the measured quantity (temperature, precipitation). The technology behind non-catching type gauges is constantly improving and having calibration and documented traceability available will support the diffusion of such systems, with direct economic and technological benefits. Together with more reliable data, this will also contribute to better environmental analyses and climate studies by enhancing data comparability (Merlone et al., 2020b).

ACKNOWLEDGEMENTS

This 18NRM03 project INCIPIT 'Calibration and accuracy of non-catching instruments to measure liquid/solid atmospheric precipitation' has received funding from the EMPIR programme co-financed by the Participating States and from the European Union's Horizon 2020 research and innovation programme.

ORCID

L. G. Lanza https://orcid.org/0000-0002-5874-0357
A. Cauteruccio https://orcid.org/0000-0002-7931-172X
E. Chinchella https://orcid.org/0000-0002-8665-9193
M. Stagnaro https://orcid.org/0000-0002-4661-7677
M. Dobre https://orcid.org/0000-0002-5193-0238
M. C. Garcia Izquierdo https://orcid.org/0000-0001-8183-1399
G. Coppa https://orcid.org/0000-0002-2847-3286
C. Musacchio https://orcid.org/0000-0001-7473-3678

REFERENCES

Atlas, D., Srivastava, R.C. & Sekhon, R.S. (1973) Doppler radar characteristics of precipitation at vertical incidence. *Reviews of Geophysics*, 11(1), 1–35.

Battaglia, A., Rustemeier, E., Tokay, A., Blahak, U. & Simmer, C. (2010) PARSIVEL snow observations: a critical assessment. *Journal of Atmospheric and Oceanic Technology*, 27(2), 333–344.

Beard, K.V. (1976) Terminal velocity and shape of cloud and precipitation drops aloft. *Journal of the Atmospheric Sciences*, 33, 851–864.

Beard, K.V. & Chuang, C. (1987) A new model for the equilibrium shape of raindrops. *Journal of the Atmospheric Sciences*, 44(11), 1509–1524.

Bernauer, F., Hürkamp, K., Rühm, W. & Tschiersch, J. (2015) On the consistency of 2-D video disdrometers in measuring microphysical parameters of solid precipitation. *Atmospheric Measurement Techniques*, 8(8), 3251–3261.

Blanchard, D.C. (1953) Raindrop size-distribution in Hawaiian rains. *Journal of Meteorology*, 10(6), 457–473.

Bringi, V.N., Chandrasekar, V. & Xiao, R. (1998) Raindrop axis ratios and size distributions in Florida rainshafts: an assessment of multiparameter radar algorithms. *IEEE Transactions on Geoscience and Remote Sensing*, 36(3), 703–715.

Caracciolo, C., Prodi, F. & Uijlenhoet, R. (2006) Comparison between Pludix and impact/optical disdrometers during rainfall measurement campaigns. *Atmospheric Research*, 82(1–2), 137–163.

Caracciolo, C., Porcu, F. & Prodi, F. (2008) Precipitation classification at mid-latitudes in terms of drop size distribution parameters. *Advances in Geosciences*, 16, 11–17.

Caton, P.G.F. (1966) A study of raindrop-size distributions in the free atmosphere. *Quarterly Journal of the Royal Meteorological Society*, 92(391), 15–30.

Cauteruccio, A. (2020) *The role of turbulence in particle-fluid interaction as induced by the outer geometry of catching-type precipitation gauges*. Ph.D. Thesis, University of Genova, Italy.

Cauteruccio, A., Colli, M., Stagnaro, M., Lanza, L.G. & Vuerich, E. (2021a) In situ precipitation measurements. In: Foken, T. (Ed.) *Springer handbook of atmospheric measurements, Part B: In-situ measurement techniques*. Switzerland: Springer Nature, p. 35.

Cauteruccio, A., Colli, M., Freda, A., Stagnaro, M. & Lanza, L.G. (2020) The Role of Free-Stream Turbulence in Attenuating the Wind Updraft above the Collector of Precipitation Gauges. *Journal of Atmospheric and Oceanic Technology*, 37(1), 103–113. https://doi.org/10.1175/jtech-d-19-0089.1.

Cauteruccio, A., Brambilla, E., Stagnaro, M., Lanza, L.G. & Rocchi, D. (2021b) Wind tunnel validation of a particle tracking model to evaluate the wind-induced bias of precipitation measurements, conditionally accepted on. *Water Resources Research*. https://doi.org/10.1002/essoar.10504288.1.

Cauteruccio, A., Brambilla, E., Stagnaro, M., Lanza, L.G. & Rocchi, D. (2021c) Experimental evidence of the wind-induced bias of precipitation gauges using particle image velocimetry and particle tracking in the wind tunnel. *Journal of Hydrology*.

Chandrasekar, V., Cooper, W.A. & Bringi, V.N. (1988) Axis ratios and oscillations of raindrops. *Journal of the Atmospheric Sciences*, 45(8), 1323–1333.

Colli, M., Lanza, L.G., La Barbera, P. & Chan, P.W. (2014) Measurement accuracy of weighing and tipping-bucket rainfall intensity gauges under dynamic laboratory testing. *Atmospheric Research*, 144, 186–194. https://doi.org/10.1016/j.atmosres.2013.08.007.

Colli, M., Lanza, L.G., Rasmussen, R. & Thériault, J.M. (2016) The Collection Efficiency of Shielded and Unshielded Precipitation Gauges. Part II: Modeling Particle Trajectories. *Journal of Hydrometeorology*, 17(1), 245–255. https://doi.org/10.1175/jhm-d-15-0011.1.

Colli, M., Stagnaro, M., Lanza, L.G., Rasmussen, R. & Thériault, J. M. (2020) Adjustments for Wind-Induced Undercatch in Snowfall Measurements Based on Precipitation Intensity. *Journal of Hydrometeorology*, 21(5), 1039–1050. https://doi.org/10.1175/jhm-d-19-0222.1.

de Moraes Frasson, R.P., Kindl da Cunha, L. & Krajewski, W.F. (2011) Assessment of the Thies optical disdrometer performance. *Atmospheric Research*, 101(1–2), 237–255.

EN 17277:2019. (2019) *Hydrometry – measurement requirements and classification of rainfall intensity measuring instruments*. Brussels, Belgium: CEN – European Committee for Standardisation.

Folland, C. K. (1988) Numerical models of the raingauge exposure problem, field experiments and an improved collector design. *Quarterly Journal of the Royal Meteorological Society*, 114(484), 1485–1516. https://doi.org/10.1002/qj.49711448407.

Förster, J., Gust, G. & Siegfried, S. (2004) A piezoelectrical rain gauge for application on buoys. *Journal of Atmospheric and Oceanic Technology*, 21, 179–193.

Green, A.W. (1975) An approximation for the shapes of large raindrops. *Journal of Applied Meteorology*, 14(8), 1578–1583.

Grossklaus, M., Uhlig, K. & Hasse, L. (1998) An optical disdrometer for use in high wind speeds. *Journal of Atmospheric and Oceanic Technology*, 15(4), 1051–1059.

Gunn, R. & Kinzer, G.D. (1949) The terminal velocity of fall for water droplets in stagnant air. *Journal of Atmospheric Sciences*, 6(4), 243–248.

Houze, R.A., Jr., Hobbs, P.V., Herzegh, P.H. & Parsons, D.B. (1979) Size distributions of precipitation particles in frontal clouds. *Journal of the Atmospheric Sciences*, 36(1), 156–162.

Jevons, W.S. (1861) On the deficiency of rain in an elevated rain-gauge, as caused by wind. *The London, Edinburgh, and Dublin Philosophical Magazine and Journal of Science*, 22(149), 421–433.

Joss, J. & Waldvogel, A. (1967) Ein Spektrograph für Niederschlagstropfen mit automatischer Auswertung. *Pure and Applied Geophysics*, 68, 240–246.

Kathiravelu, G., Lucke, T. & Nichols, P. (2016) Rain drop measurement techniques: a review. *Water*, 8(1), 29.

Kinnel, P.I.A. (1972) The acoustic measurement of water-drop impacts. *Journal of Applied Meteorology*, 11, 691–694.

Kourtellis, A.G., Kasparis, T., Jones, L. & Lane, J. (2005) Disdrometer calibration using an adaptive signal processing algorithm. In: *Proceedings of OCEANS 2005 MTS/IEEE*. Washington, DC: IEEE.

Kruger, A. & Krajewski, W.F. (2002) Two-dimensional video disdrometer: A description. *Journal of Atmospheric and Oceanic Technology*, 19(5), 602–617.

Lanza, L. G. & Stagi, L. (2008) Certified accuracy of rainfall data as a standard requirement in scientific investigations. *Advances in Geosciences*, 16, 43–48. https://doi.org/10.5194/adgeo-16-43-2008.

Lanzinger, E., Manfred, T. & Herbert, W. (2006) *Rainfall amount and intensity measured by the Thies laser precipitation monitor*. TECO-2006, Geneva, Switzerland.

Licznar, P., Łomotowski, J., Błoński, S. & Ciach, G.J. (2008) Microprocessor field impactometer calibration: do we measure drops' momentum or their kinetic energy? *Journal of Atmospheric and Oceanic Technology*, 25(5), 742–753.

Löffler-Mang, M., Kunz, M. & Schmid, W. (1999) On the performance of a low-cost K-band Doppler radar for quantitative rain measurements. *Journal of Atmospheric and Oceanic Technology*, 16(3), 379–387.

Löffler-Mang, M., Schön, D. & Landry, M. (2011) Characteristics of a new automatic hail recorder. *Atmospheric Research*, 100(4), 439–446.

Löffler-Mang, M. & Joss, J. (2000) An optical disdrometer for measuring size and velocity of hydrometeors. *Journal of Atmospheric and Oceanic Technology*, 17(2), 130–139.

Marshall, J.S., Langille, R.C. & Palmer, W.M.K. (1947) Measurement of rainfall by radar. *Journal of Meteorology*, 4(6), 186–192.

Marshall, J.S. & Palmer, W.M. (1948) K: the distribution of raindrops with size. *Journal of Meteorology*, 5(4), 165–166.

Merlone, A., Lopardo, G., Sanna, F., Bell, S., Benyon, R., Bergerud, R.A. et al. (2015) The MeteoMet project – metrology for meteorology: challenges and results. *Meteorological Applications*, 22, 820–829. https://doi.org/10.1002/met.1528.

Merlone, A., Lopardo, G., Sanna, F., Bell, S., Benyon, R., Bergerud, R. A., et al. (2015) The MeteoMet project - metrology for meteorology: challenges and results. *Meteorological Applications*, 22, 820–829. https://doi.org/10.1002/met.1528.

Merlone, A., Coppa, G., Musacchio, C., Lanza, L.G., Cauteruccio, A., Stagnaro, M., et al. (2020a) The INCIPIT project: calibration and accuracy of non-catching instruments to measure liquid/solid atmospheric precipitation. In: *WMO/CIMO Technical Conference on Meteorological and Environmental Instruments and Methods of Observation (CIMO TECO-2020)*. Paris, France, 21–24 September 2020.

Merlone, A., Coppa, G., Musacchio, C., Lanza, L.G., García Izquierdo, C., Roulet, Y.-A., et al. (2020b) Metrological traceability to improve data comparability. In: *WMO data conference – earth system data exchange in the 21st century*. 16–18 November 2020, Geneva, Switzerland.

Mueller, E. (1965) *Radar rainfall studies*. Doctoral dissertation, Ph. D. dissertation, University of Illinois.

Nešpor, V. & Sevruk, B. (1999) Estimation of wind-induced error of rainfall gauge measurements using a numerical simulation. *Journal of Atmospheric and Oceanic Technology*, 16(4), 450–464. https://doi.org/10.1175/1520-0426(1999)016%3C0450:EOWIEO%3E2.0.CO;2.

Nitu, R., Roulet, Y.-A., Wolff, M., et al. (2018) *WMO solid precipitation intercomparison experiment (SPICE) (2012–2015)*. World Meteorological Organisation, Instruments and Observing Methods (IOM) Report No. 131, pp. 1445.

Prodi, F., Tagliavini, A. & Medini, R. (2000) Time variability in rainfal events observed by Pludix. *Physics and Chemistry of the Earth, Part B: Hydrology, Oceans and Atmosphere*, 25(10–12), 959–963.

Pruppacher, H.R. & Beard, K.V. (1970) A wind tunnel investigation of the internal circulation and shape of water drops falling at

terminal velocity in air. *Quarterly Journal of the Royal Meteorological Society*, 96(408), 247–256.

Pruppacher, H.R. & Pitter, R.L. (1971) A semi-empirical determination of the shape of cloud and rain drops. *Journal of the Atmospheric Sciences*, 28(1), 86–94.

Rasmussen, R.M., Vivekanandan, J., Cole, J., Myers, B. & Masters, C. (1999) The estimation of snowfall rate using visibility. *Journal of Applied Meteorology*, 38(10), 1542–1563.

Rauber, R.M. & Nesbitt, S.W. (2018) *Radar meteorology: a first course*. Hoboken, NJ: John Wiley & Sons.

Salmi, A., Ikonen, J. & Oyj, V. (2005) Piezoelectric precipitation sensor from Vaisala. In: *WMO technical conference on instruments and methods of observation (TECO-2005)*, Bucharest, Romania, May 2005. pp. 4–7.

Salmi, A., Elomaa, L., Kopsala, P. & Laukkanen, E. (2011) Piezoelectric Vaisala raincap® rain sensor applied to drop size distribution monitoring. In: *Technical Conference on Meteorological and Environmental Instruments and Methods of Observation*. Geneva: World Meteorological Organization, pp. 1–7.

Santana, M.A.A., Guimarães, P.L.O., Lanza, L.G. & Vuerich, E. (2015) Metrological analysis of a gravimetric calibration system for tipping-bucket rain gauges. *Meteorological Applications*, 22, 879–885. https://doi.org/10.1002/met.1540.

Sheppard, B.E. (1990) Measurement of raindrop size distributions using a small Doppler radar. *Journal of Atmospheric and Oceanic Technology*, 7(2), 255–268.

Sheppard, B.E. (1996) Effect of rain on ground-based microwave radiometric measurements in the 20–90-GHz range. *Journal of Atmospheric and Oceanic Technology*, 13(6), 1139–1151.

Smith, C.D., Ross, A., John Kochendorfer, J., Earle, M.E., Wolff, M., Buisán, S. et al. (2020) Evaluation of the WMO solid precipitation intercomparison experiment (SPICE) transfer functions for adjusting the wind bias in solid precipitation measurements. *Hydrology and Earth System Sciences*, 24, 4025–4043.

Szakall, M., Diehl, K., Mitra, S.K. & Borrmann, S. (2009) A wind tunnel study on the shape, oscillation, and internal circulation of large raindrops with sizes between 2.5 and 7.5 mm. *Journal of the Atmospheric Sciences*, 66(3), 755–765.

Testik, F.Y. & Rahman, M.K. (2016) High-speed optical disdrometer for rainfall microphysical observations. *Journal of Atmospheric and Oceanic Technology*, 33(2), 231–243.

Thériault, J.M., Rasmussen, R., Ikeda, K. & Landolt, S. (2012) Dependence of snow gauge collection efficiency on snowflake characteristics. *Journal of Applied Meteorology and Climatology*, 51, 745–762. https://doi.org/10.1175/JAMC-D-11-0116.1.

Thériault, J.M., Rasmussen, R., Petro, E., Trépanier, J.Y., Colli, M. & Lanza, L.G. (2015) Impact of wind direction, wind speed, and particle characteristics on the collection efficiency of the double fence intercomparison reference. *Journal of Applied Meteorology and Climatology*, 54(9), 1918–1930. https://doi.org/10.1175/JAMC-D-15-0034.1.

Thies-Clima. (2011) *Laser precipitation monitor V2.5x STD. instruction for use (0213441/07/11)*. Göttingen, Germany: Adolf Thies GmbH & Co., p. 66.

Tuukka, P. (2015) *Calibration of non-catching precipitation sensors (Vaisala)*. MeteoMet2 workshop, Genova University, March 11th–12th.

Ulbrich, C.W. (1983) Natural variations in the analytical form of the raindrop size distribution. *Journal of Climate and Applied Meteorology*, 22(10), 1764–1775.

UNI 11452. (2012) *Hydrometry – Measurement of rainfall intensity (liquid precipitation) – Metrological requirements and test methods for catching type gauges*. Milan, Italy: UNI – Ente Nazionale Italiano di Unificazione.

Vuerich, E., Monesi, C., Lanza, L.G., Stagi, L. & Lanzinger, E. (2009) *WMO field intercomparison of rainfall intensity gauges*. World Meteorological Organisation – Instruments and Observing Methods Rep. No. 99, WMO/TD No. 1504, pp. 286.

Waldvogel, A. (1974) The N_0 jump of raindrop spectra. *Journal of the Atmospheric Sciences*, 31(4), 1067–1078.

WMO Guide to Meteorological Instruments and Methods of Observation. (2018) WMO-N.8. ISBN 978-92-63-10008-5. Available at: https://library.wmo.int/doc_num.php?explnum_id=10616 [Accessed 14/05/2021].

WMO Solid Precipitation Intercomparison Experiment (SPICE). (2012–2015) IOM 131-2018. Available at: https://library.wmo.int/doc_num.php?explnum_id=5686 [Accessed 14/05/2021].

How to cite this article: Lanza, L. G., Merlone, A., Cauteruccio, A., Chinchella, E., Stagnaro, M., Dobre, M., Garcia Izquierdo, M. C., Nielsen, J., Kjeldsen, H., Roulet, Y. A., Coppa, G., Musacchio, C., Bordianu, C., & Parrondo, M. (2021). Calibration of non-catching precipitation measurement instruments: A review. *Meteorological Applications*, *28*(3), e2002. https://doi.org/10.1002/met.2002